The morphology of simulated trade-wind congestus clouds under wind shear

K. C. Helfer[1], L. Nuijens[1]

[1]Department of Geoscience and Remote Sensing, Delft University of Technology, Delft, The Netherlands

Key Points:

- Without cold pools, new convection is triggered upwind of existing cells.
- In the absence of (or only weak) subcloud-layer shear, rain falls into emerging updrafts, hindering convective development.
- Forward shear (increasing wind speed) in the subcloud layer enhances uplift at cold-pool boundaries, favouring the triggering of convection.

Corresponding author: Kevin Helfer, `k.c.helfer@tudelft.nl`

Abstract

Intrigued by a growing body of research on convective organisation, this study investigates the morphology of precipitating marine cumulus convection with and without cold pools under vertical wind shear. We ran idealised large-eddy-simulation experiments with zonal forward and backward shear and without shear. Without (or only weak) subcloud-layer shear, conditions are unfavourable for convective deepening, as clouds remain stationary relative to their subcloud-layer roots, and precipitative downdrafts interfere with emerging updrafts. Conversely, under forward shear, where the wind strengthens with height (a condition that is commonly found in the trades), clouds move at a faster speed than their roots, and precipitation falls downwind away from emerging updrafts. This significantly facilitates convective deepening, precipitation and consequently the formation of cold pools. Forward shear has another advantage as opposed to weak or backward shear: The existing background vorticity interacts with the (opposing) vorticity of cold-pool gust fronts which facilitates forced uplift. Inhibiting cold-pool formation delays convective deepening only shortly.

Plain Language Summary

The most common type of clouds in Earth's trade wind-regions is so-called gravel: relatively unorganised precipitating clouds of medium depth. The precipitation of such clouds can cause so-called cold pools: cold air that spreads out laterally near the surface in a circular fashion triggering new clouds in arc-like patterns. We used a high-resolution weather model to investigate how the morphology of such gravel clouds and the associated cold pools is affected by vertical changes in the wind speed (shear). When the wind speed at the surface and at cloud base is the same, clouds remain above their 'roots', and downward-moving air associated with rain falls into those cloud roots, which hinders the further development of the cloud field. Conversely, when the wind speed increases from the surface to cloud base (which it often does), clouds move away from their roots and thus do not rain onto them, allowing for the development of deeper clouds. Formation of new clouds at the edge of cold pools depends on the shear too. Even when we artificially inhibit the development of cold pools, deep clouds still develop, confirming that cold pools are not crucial for the transition from shallow to deep marine clouds.

1 Introduction

Triggered by the World Climate Research Programme's grand challenge on clouds, circulation and climate sensitivity (Bony et al., 2015), tremendous research efforts have been undertaken in recent years to study maritime shallow clouds, with an increasing interest in their organisation. A culmination was the EUREC^{4}A field campaign in 2020 (Stevens et al., 2021, in review), which also motivated the successful classification of trade-wind cloud patterns by their visual appearance from space into classes called fish, flower, sugar and gravel (Stevens et al., 2019). The dominant pattern of trade-wind convection is not the unorganised, non-precipitating cumulus humilis cloud (sugar) but rather the somewhat deeper, precipitating congestus (gravel) that may have a stratiform outflow (flower) at greater heights (Schulz et al., 2021, in review). This finding motivates us to shed more light specifically on cumulus congestus clouds from large-eddy simulations (LES): simulations that differ from the traditional BOMEX and ATEX cases that have been intensely used in the past decades (Nuijens & Siebesma, 2019).

Surface wind speed (and to lesser extent wind shear) is considered as one of the predictors of the aforementioned cloud patterns (Bony et al., 2020; Schulz et al., 2021, in review). Helfer et al. (2020) (hereafter: HNRS20) ran idealised large-eddy simulations (LES) to investigate the effect of wind shear on trade-wind cumulus convection, differentiating between backward shear (BS), where surface winds weaken with height, and forward shear (FS), where surface winds strengthen with height. Indicative of their representativeness of the trades, these simulations are dominated by clouds that resemble gravel and (at times) flowers. A main result of HNRS20's study is that any wind shear limits the strength of cloud updrafts because of a stronger downward-oriented pressure perturbation force (as found in studies of deep convection, e.g. Peters et al., 2019). As a consequence cloud deepening is hampered in the presence of shear. However, under FS, convection appears to have a tendency to grow deeper, which seems related to their enhanced potential to aggregate moisture on mesoscales. Another intriguing observation of HNRS20 is that wind anomalies found within cold pools depend on the direction of the shear. This may hint at a possible role of downdrafts introducing different cloud-layer momentum in the surface and subcloud layers. In modelling studies of deep convective cold pools, convective momentum transport (CMT) has been found to significantly influence cold-pool winds (Mahoney et al., 2009; Grant et al., 2020). HNRS20 speculated about the possible role of triggering secondary convection at cold-pool edges in the convection's response to wind shear.

Two main mechanism are being discussed in the literature as to how cold pools trigger new convection (Torri et al., 2015): one purely thermodynamic mechanism (Tompkins, 2001; Seifert & Heus, 2013) and one by dynamic lifting at the cold-pool edges (Xue et al., 2008; Böing et al., 2012; Li et al., 2014). Using a cloud-resolving model, Tompkins (2001) showed that during the development of deep convective cold pools, evaporation of precipitation already cools and moistens the boundary layer before a downdraft develops that cools and dries the boundary layer. The cold pools's gust front is consequently moister than the cold-pool centre. The lowered temperature can quickly recover, which close to removes all convective inhibition (CIN), allowing for new convection due to even minimal lifting. In their LES study of a specific RICO day, Li et al. (2014) found little evidence that supports Tompkins' thermodynamic hypothesis for shallow convection. Inspired by studies on mid-latitude squall lines (Rotunno et al., 1988; Weisman & Rotunno, 2004), they particularly pointed out a possible role of near-surface wind shear in the dynamic triggering of further convection. In their case, the vorticity of the cold-pool boundary is weaker than that of the ambient wind profile, and convection thus tilts away from the cold pool, gaining access to converged moisture, which is advantageous for cloud growth. Hence, it seems plausible that this process could help explain differences between FS and BS. After all, cold pools have also been shown to play a crucial role in the deepening of convection over land (Khairoutdinov & Randall, 2006; Böing et al., 2012; Schlemmer & Hohenegger, 2014; Kurowski et al., 2018).

Compelled by the findings of HNRS20, our objective in the present study is to address why cloud deepening is inhibited more under FS than under BS and what role cold-pool organisation plays in this. We describe the morphology of shallow convective systems under shear in idealised large-domain LESs with and without the evaporation of precipitation. By turning off evaporation, we limit the formation of cold pools and are enabled to study both unorganised convection and cold-pool dynamics. By utilising a computational domain of 50×50 km^2, we are mindful of the lack of organisation in conventional LES domains, which remains a challenge to address (Nuijens & Siebesma, 2019).

The remainder of this paper is structured as follows. In the following section, we shortly review the simulation set-up as well as the additional simulations we ran for the

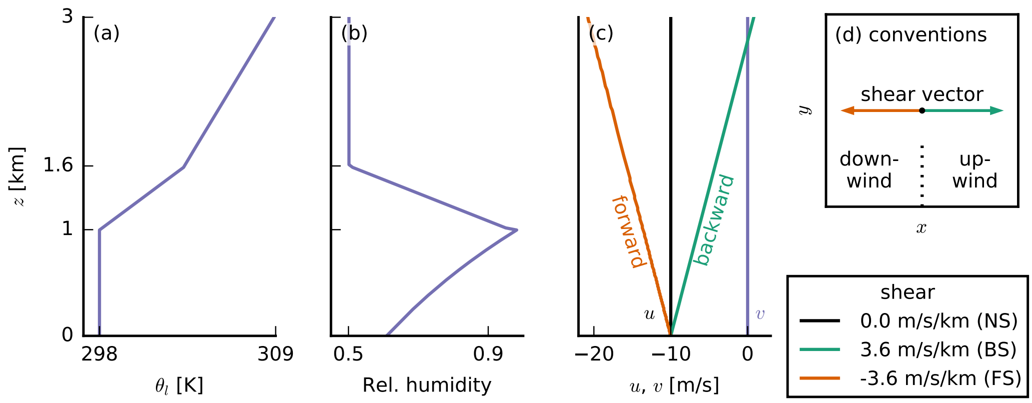

Figure 1: Initial profiles of (a) liquid water potential temperature θ_l, (b) relative humidity and (c) the two wind components u and v. Purple profiles are the same in all simulations. Orange stands for forward shear (FS), black for no shear (NS) and green for backward shear (BS). This colour coding is the same for all other figures. (d) Schematic of the directional conventions used in this paper: downwind is in the negative x-direction, upwind in the positive x-direction.

present paper. We then present the results in a twofold manner. First, we discuss the effects of wind shear on cold pools and the triggering of new convection at their fronts. Second, we ask how clouds behave under wind shear before cold pools emerge, by analysing simulations in which cold-pool formation is suppressed. Finally, we discuss and summarise our findings in a concluding section.

2 Experimental design

We utilised the same experimental set-up as in HNRS20 and only point out its most important aspects here. Using version 4.2 of the Dutch Atmospheric Large-Eddy Simulation model (DALES; Heus et al., 2010), we simulated an idealised shallow cumulus case, typical of the North Atlantic trades (Fig. 1). Our domain has a size of $50.4 \times 50.4 \times 17.9$ km^3, with a resolution of 100 m in the horizontal and a non-uniform vertical grid (resolution stretched from 10 m at the surface to 190 m at the top). Simulations were run for 48 h, to allow for the development of sufficient precipitation. Advection was computed by a 5th-order scheme in the horizontal and a 2nd-order scheme in the vertical, and a Galilean transform was performed to reduce advective errors. We deployed a single-moment ice microphysics scheme that allows for precipitation (Grabowski, 1998).

For the sensible and latent surface heat fluxes, we prescribed $SHF = 15.3$ W m^{-2} and $LHF = 225.2$ W m^{-2}, respectively. These values allow for the development of somewhat deeper congestus clouds, which we are interested in. By keeping the fluxes fixed, we maintain a good comparability among our simulations, even when convection in some of them gets deeper and surface feedbacks would occur with in interactive surface scheme. While over land interactive surface enthalpy fluxes are crucial for cold-pool modelling, Gentine et al. (2016) suggest that over oceans they only matter for cold pools of scales much larger than our domain. The surface momentum flux was computed interactively by the model. We applied a constant radiative cooling rate of -2.5 K/d to the liquid water potential temperature θ_l. Large-scale subsidence was calculated interactively, using a weak-temperature-gradient approach (WTG; Daleu et al., 2012). The total water specific humidity q_t was nudged towards its initial profile above 4 km with a time scale of 6 h to avoid spurious moisture tendencies.

To investigate the dependence of shallow convection and cold pools on vertical wind shear, we ran experiments with different wind profiles (Fig. 1c). As discussed by HNRS20, backward shear, where surface easterlies weaken with height and turn westerlies eventually, is by far the most common in the North Atlantic trades. However, forward shear, where surface easterlies strengthen with height, occasionally occurs as well, in particular in July and August. The analysis of HNRS20 shows distinct differences in the effect that shear has on convection when it is forward as opposed to backward. They further show that the strength of shear does not play a major role. Hence, we investigated three different zonal wind profiles with either no shear (NS, black line in Fig. 1c), backward shear (BS, green, $\partial_z u = 3.6 \times 10^{-3}$ s^{-1}) or forward shear (FS, orange, $\partial_z u = -3.6 \times 10^{-3}$ s^{-1}). (Note that our BS and FS cases correspond to the BS-4X and FS-4X cases of HNRS20, respectively.) These wind profiles were used as both the initial profiles and the geostrophic forcing. We did not prescribe any meridional wind (purple line in Fig. 1c).

In addition to one set of standard runs with each of the three wind profiles (labelled STD), we performed another set of experiments in which we suppressed the formation of cold pools (labelled NCP, no cold pools). To this end, we turned off the evaporation of precipitation in the LES, which Böing et al. (2012) showed to be very effective. All precipitation in these simulations reaches the surface, and no latent cooling due to the evaporation of rain occurs, which is a crucial ingredient for the formation of cold pools (e.g. Khairoutdinov & Randall, 2006).

3 Cold pools under shear

All our standard simulations (STD) are characterised by the gravel type of organisation including cold pools (Fig. 2). In Fig. 2, we present top-down views of the computational domain, showcasing the different structure of cold pools in our three shear cases. In these snapshots, the mean wind ($\sim u$) blows from right to left, and hence, the left is referred to as downwind and the right as upwind (see also Fig. 1d). We remark that in the context of the trades where wind blows from east to west, one can think of Fig. 2 as views with north at the top.

Cold-pool formation starts with the precipitative downdraft (rain shaft) of a deep cloud, at least in the case of cumuli-form clouds. Upon arrival at the surface, the dense air mass spreads out laterally as a gravity current, which is reflected by the diverging wind patterns shown in Fig. 2a–c. In those snapshots, red areas have (total) wind speeds faster than the slab average and are most prominently found at the downwind front of the cold pool. Since this gust front moves in the same direction as the mean wind, velocities add up, leading to faster-than-average wind speeds. Conversely, on the upwind side of the cold pools, the cold-pool front moves against the mean wind, leading to slower total wind speeds (shown in blue).

The cold pools have a characteristic thermodynamic signature (Fig. 2d–f). The downdraft air first tends to be moist and cold (due to its origin at high altitudes and the evaporation of precipitation). This is reflected in a relatively high equivalent potential temperature θ_e (which contains information about both the temperature and the relative humidity) in the outermost regions of the cold pools (Fig. 2d–f). Later on in its evolution, when precipitation ceases, the downdraft stays cold but becomes drier, resulting in a low θ_e in the cold-pool centre. While in the NS and FS cases, cold pools of significant size and strength occur (like the ones in Fig. 2a and b), they are much smaller in the BS case (Fig. 2c). As we will later elaborate, they also occur more rarely in the BS and the FS cases. Visual inspection of a large number of scenes from our simulations suggests that new convection (strong subcloud-layer updrafts indicated in green in Fig. 2)

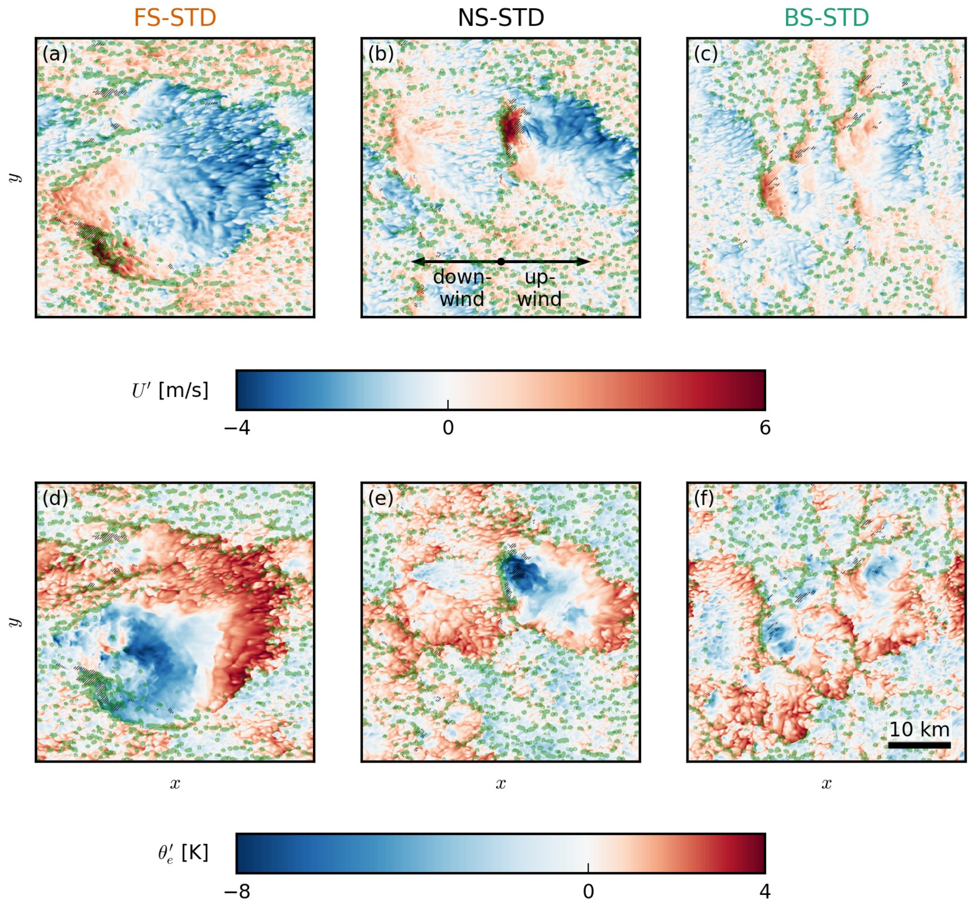

Figure 2: Snapshots of the LES domains during exemplary cold-pool events in the (a, d) FS-STD, (b, e) NS-STD and (c, f) BS-STD case. The colourmaps in the x-y cross section show (a–c) equivalent potential temperature deviations θ_e' and (d–f) total wind speed deviations U' (both from the slab average) at the lowest model level (5 m). The green outlines indicate strong updrafts in the subcloud layer ($w = 1$ m/s at 400 m), and the hatched areas indicate surface precipitation ($q_r > 0$). The snapshots were taken around 40 h.

is preferably triggered at the downwind edge of the cold pools (i.e. on the left in the panels of Fig. 2), forming arcs of shallow clouds.

We further investigate the particular cold pools from Fig. 2, focusing on their downwind sides where convection is preferably triggered. In each panel in Fig. 3, the strong precipitative downdraft of the cold pool is located near the right edge of the excerpt (see Fig. 3a, e, i). Focusing on the NS-STD case (middle row), the cold pool itself is visible as a low-temperature tongue (in terms of equivalent potential temperature θ_e) extending from the right edge of the snapshot to nearly the 1-km mark (Fig. 3f). It is there that new updrafts and clouds (secondary convection) are forming (Fig. 3e). An important ingredient in the triggering of new convection by cold-pools is the convergence that occurs at its fronts (near $x = 1$ km in Fig. 3g). Horizontal convergence, $C_h = -\partial_x u - \partial_y v$, occurs at both the upwind and the downwind front, but only the downwind front is additionally characterised by a vorticity contrast that aids forced lifting. Considering the meridional component of vorticity, $\omega_y = \partial_z u - \partial_x w$, we find that within the gravity current (i.e. right of the 1-km mark in Fig. 3h) the (zonal) wind speed increases with height (because the current is strongest near the surface), resulting in positive vorticity. The environment, however, is characterised by forward shear in the surface layer and thus negative vorticity (left of 1 km in Fig. 3h). This leads to the aforementioned vorticity contrast at the downwind edge of the cold pool that aids mechanical lifting of air parcels at this location (Fig. 3e; also see Fig. 11d for a conceptual sketch) and thus triggers new convection (Li et al., 2014).

In the above discussion of secondary convection, we highlighted the NS case, but the same processes occur in the BS and FS cases too (Fig. 3). However, Li et al. (2014) pointed out that the vorticity contrast at the cold-pool front is dependent on the background wind profile and thus generally more pronounced under forward shear (Fig. 3d). In our simulations, near-surface forward shear is present in all cases (and mostly so in the FS and NS cases), as winds are slowed down in the mixed layer towards the surface (solid lines in Fig. 4a). In the BS case, the near-surface shear is weaker and extends over a thinner layer. Locally, positive vorticity is a common feature of the downwind side of cold pools in all cases (as illustrated in Fig. 3d, h, l). However, only in the NS case, the profile of ω_y is positive when it is averaged over the whole downwind side of cold pools (Fig. 4b). Although Fig. 4b reveals that ω_y is generally less negative on the downwind

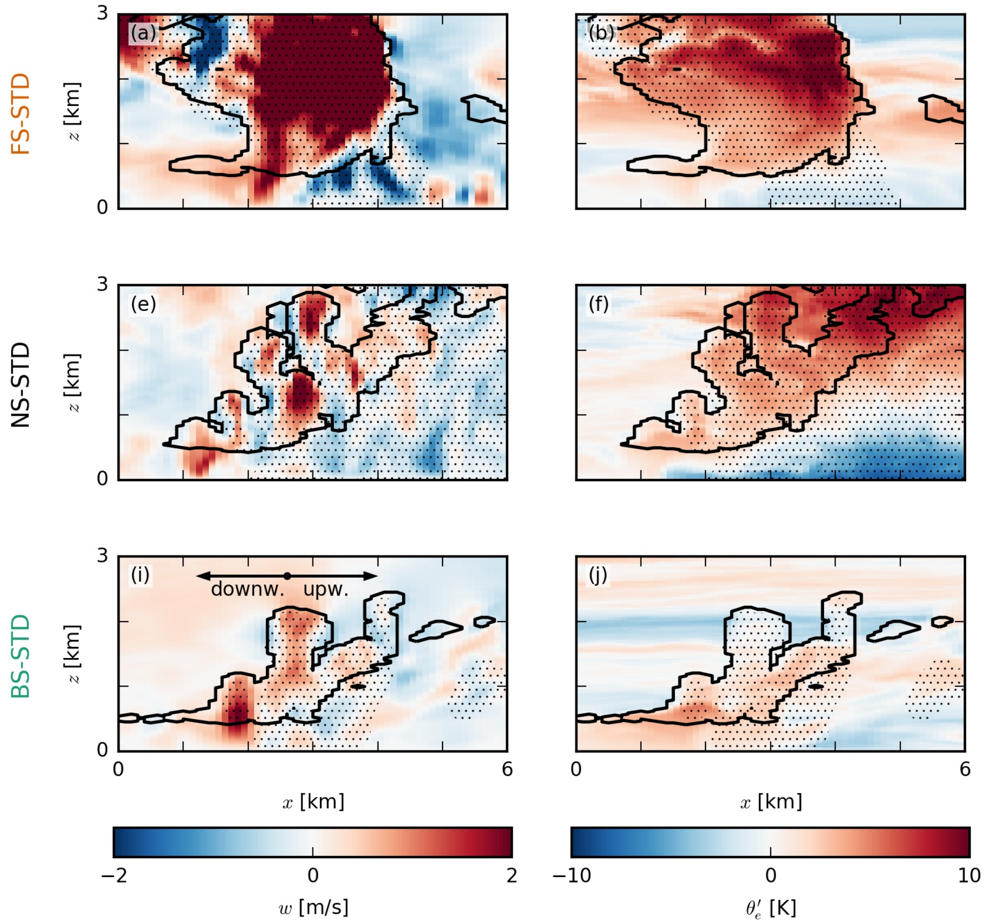

Figure 3: Snapshots of exemplary cold-pool fronts in the (a–d) FS-STD, (e–h) NS-STD and (i–l) BS-STD cases. The colourmaps in the x-z slices show (left column) the vertical velocity w and (right column) the equivalent potential temperature anomaly θ_e'. In each panel, the black outlines indicate clouds (i.e. the $q_l = 0$ isoline), the dotted areas indicate precipitation. Each panel is 6 km wide, averaged over 1 km in the meridional direction and taken from around 40 h (the same times as Fig. 2).

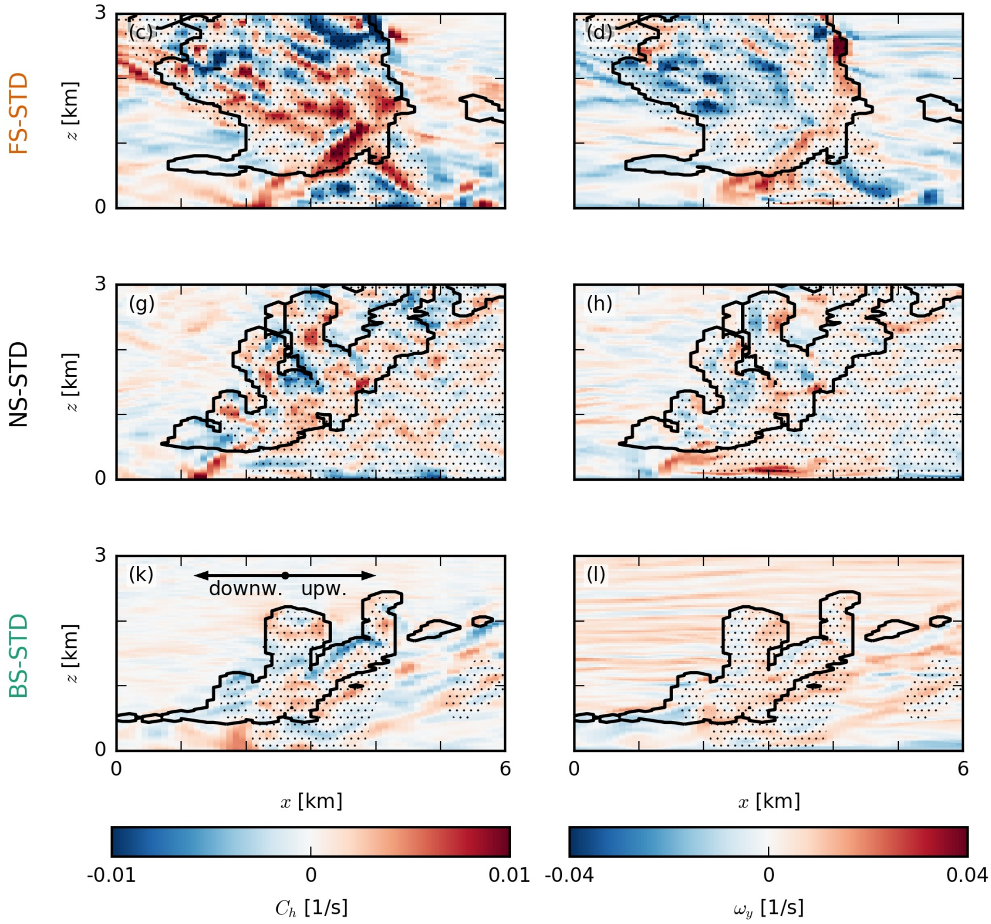

Figure 3: (continued) The colourmaps in the x-z slices show (left column) the horizontal convergence C_h and (right column) the meridional component of the vorticity ω_y.

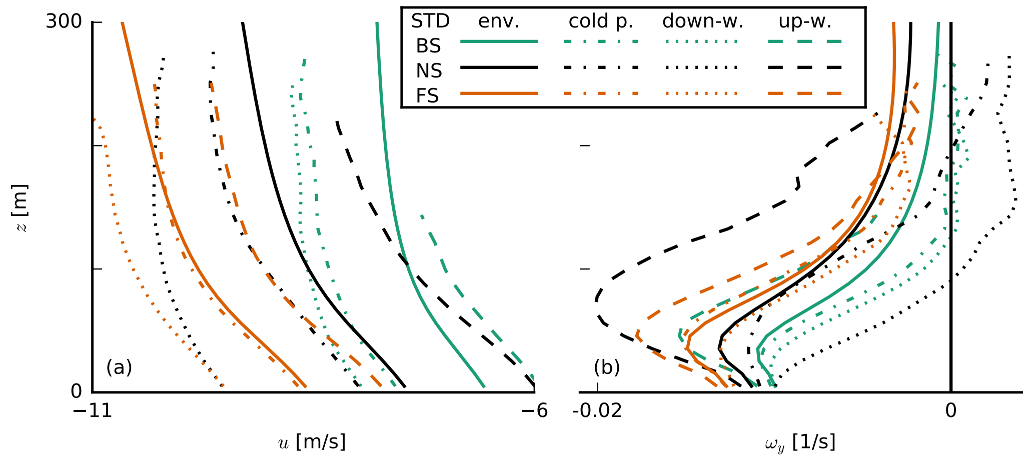

Figure 4: Profiles of (a) zonal wind speed u and (b) meridional vorticity ω_y sampled over cold pools ($\theta_l' < -0.5$ K and $q_t' < 0$; dotted-dashed), positive wind anomalies ($U' > 0$, downwind) within cold pools (dotted), negative wind anomalies ($U' < 0$, upwind) within cold pools (dashed) and the environment (solid lines), all averaged over the last ten hours of the STD simulations. As explained in Fig. 1, orange indicates forward shear (FS), black no shear (NS) and green backward shear (BS).

side than the upwind side of cold pools (and the environment), this suggests that the development of secondary convection is particularly pronounced in the NS case.

To shed more light on the above mentioned patterns of convergence and vorticity, we present probability density functions (PDFs) in Fig. 5. We remark that these PDFs are sampled over the entire domain, but sampling only within cold pools brings the same signals to light as the ones we discuss in the following (not shown). First, we find indications of more pronounced cold pools in the FS and NS cases: The PDF of subcloud-layer equivalent potential temperature shows significant occurrences of low θ_e' (Fig. 5a), and the PDF of horizontal convergence and divergence (Fig. 5b) shows that much stronger divergence occurs in these cases. Both these cases also have stronger subcloud-layer updrafts and downdrafts (Fig. 5c) and more surface precipitation (Fig. 5d). The PDF of the meridional vorticity component (Fig. 5e) shows more pronounced negative tails in the FS- and NS-STD cases, indicative of the negative vorticity due to the background forward shear in the subcloud layer. Due to the lack of subcloud shear under BS, the tail is much less pronounced in this case. The other side of the PDF indicates positive vor-

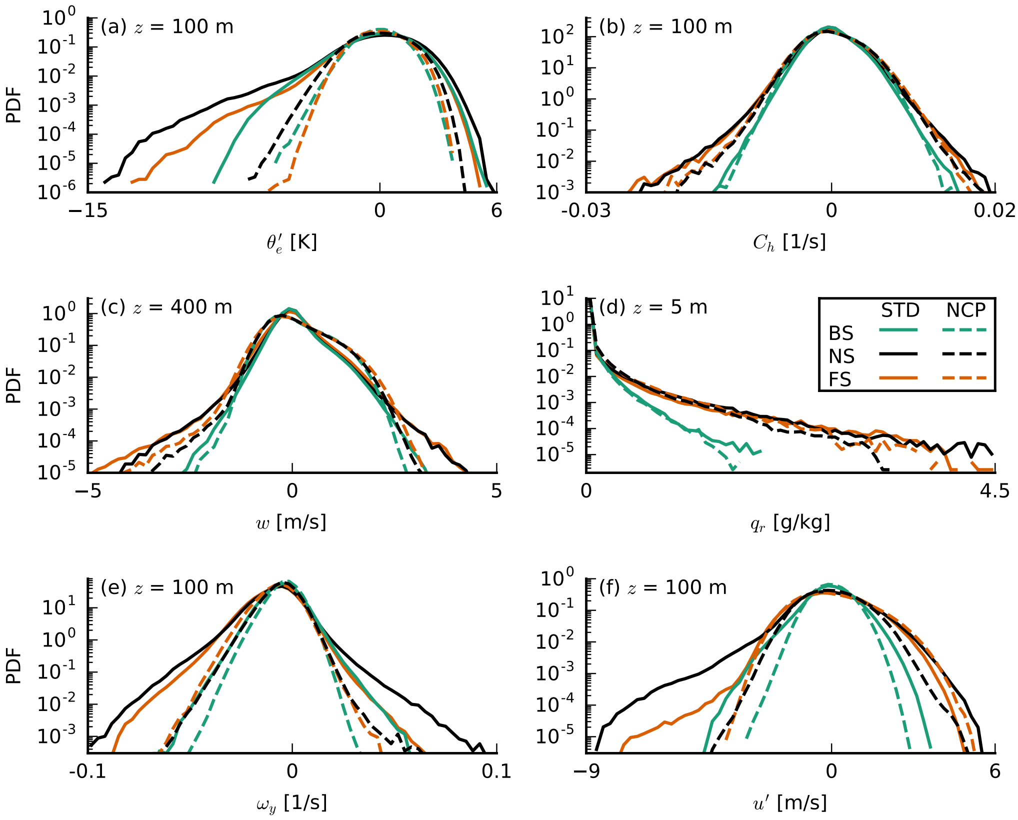

Figure 5: Probability density functions (PDFs) of (a) the equivalent potential temperature anomaly θ'_e at 100 m, (b) the horizontal convergence C_h at 100 m, (c) the vertical velocity w at 400 m, (d) the rain water specific humidity q_r at 5 m, (e) the meridional vorticity component ω_y at 100 m and (f) the zonal wind speed anomaly u' at 100 m, all averaged over the last ten hours of each simulation. Solid lines indicate the standard simulations (STD) and dashed lines the no-cold-pools simulations (NCP). As explained in Fig. 1, orange indicates forward shear (FS), black no shear (NS) and green backward shear (BS). The line colours and types are the same in all following figures, unless indicated otherwise.

ticity as it can be found within the downwind cold-pool tongue, which is only pronounced in the NS-STD case. This again suggests differences in the dynamical triggering of new convection via cold pools in our three shear cases — an observation we will come back to below.

Not only the dense air mass created by evaporation of precipitation, but also CMT can play a role in regulating the gust front. Differences in the near-surface wind-speed structure are shown in Fig. 5f (and also evident in Fig. 2a–c): Positive wind-speed anomalies (faster wind at the downwind cold-pool front) seem to be significantly stronger than negative anomalies (slower wind at the upwind front), in particular in the NS and FS cases. In other words, the cold pools are not symmetric. CMT might play a role here: Several recent studies of deep convective cold pools suggest that the precipitative downdraft that causes the cold pool also transports momentum downward that significantly influences the wind within the cold pool (Mahoney et al., 2009; Grant et al., 2020). For example, in a case with strong forward shear — like our FS and to lesser extent our NS cases —, CMT will transport faster momentum to the surface leading to faster wind in the downwind cold-pool front. Figure 5f shows such a signature of strong negative u anomalies in the FS and the NS case, which, in addition to the fact that cold pools are stronger in these cases (Fig. 5a), may be attributable to CMT.

We remind the reader that our simulations were run with constant surface fluxes to ensure that differences in surface wind speed that develop due to shear and momentum transport do not cause even larger differences in cloud and boundary-layer depth. Prescribed fluxes also inhibit thermodynamic responses, which implies that the observed differences in forced uplift (Fig. 5c) are not caused by thermodynamic fluxes. Even when we repeat our experiments with an interactive surface-flux scheme and a constant sea-surface temperature (not shown), most of the aforementioned signals remain the same (e.g. cold-pool fraction as well as vorticity and wind-speed patterns). However, the comparability is somewhat limited because interactive surface fluxes in the present simulations set-up lead to deeper convection (HNRS20) and thus inherently stronger cold pools.

The stronger cold pools in the NS and FS cases are also seen in the time series of cold-pool fraction (shown in Fig. 6a as the area fraction where $\theta_l' < -0.5$ K and $q_l' < 0$ at the lowest model level). This also reveals a less common occurrence of cold pools in the FS case compared to the NS case. Sampling the PDFs of ω_y and u' only over the

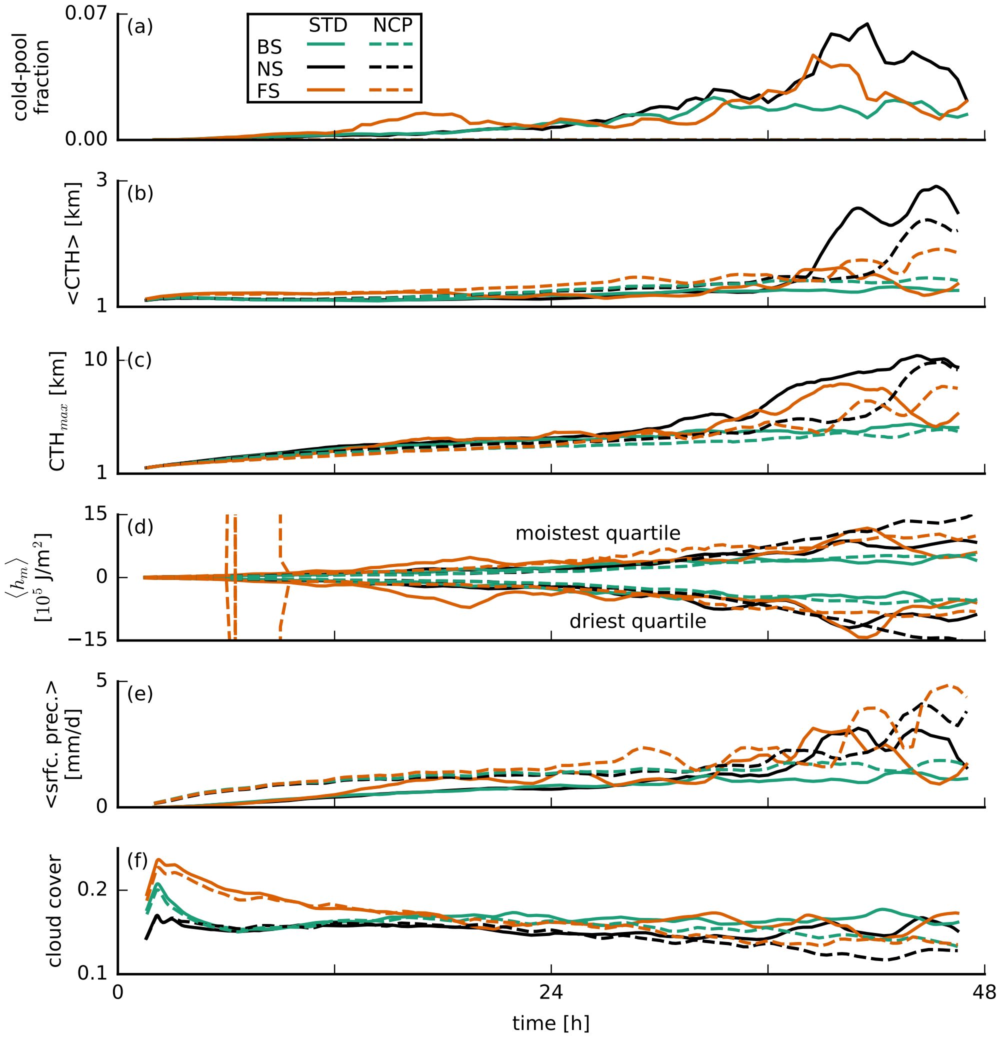

Figure 6: Time series of (a) the area fraction of cold pools ($\theta_l' < -0.5$ K and $q_t' < 0$) at the lowest model level, (b) average and (c) maximum cloud top height (CTH), (d) vertically integrated (up to 1 km) moist static energy anomalies $< h_m >$ in the moistest and driest quartiles of 12.6×12.6 km^2 blocks, (e) surface precipitation and (f) cloud cover. The data are smoothed using a 3-hour running-average filter.

time when a significant cold pool is observed in the FS-NCP case too (e.g. 38–39 h, see Fig. 6a), leads to a similarly extreme positive tail in the vorticity PDF and a negative tail in the zonal-wind PDF that is even more extreme than in the NS case (not shown). However, the low statistical weight of this single, short-lived cold-pool event does not lead to a clear signature in the PDFs presented in Fig. 5, which are averaged over a longer period (38–48 h).

An important conclusion from the discussion so far is the apparent disadvantage of the BS case for the development of secondary convection. However, it has to be pointed out that the above comparison may not be entirely fair because after 40 h of simulation, convective depths differ among the three shear cases, which motivates us to also investigate time-series statistics (Fig. 6). They reveal a strong connection between convective depth, moisture aggregations, precipitation and cold pools (see also HNRS20). Deeper clouds (Fig. 6b, c) go along with stronger moisture aggregations (Fig. 6d) and cause more precipitation (Fig. 6e) and thus the formation of cold pools (Fig. 6a). Especially the second simulation day of the FS and NS cases is characterised by the regular occurrence of deeper convection and cold pools. On the other hand, the BS case does not develop any deep clouds and thus also no strong precipitation events and smaller cold pools, being at a disadvantage already in the earlier stages of the simulation.

Thus, there must be another mechanism that disadvantages the BS case, even before triggering of secondary convection at cold-pool edges starts to play a role. We will shed more light on this in the following section where we discuss our simulations in which cold pools are suppressed (NCP).

4 Sheared convection before cold pools

4.1 System development without evaporation of precipitation

Turning off the evaporation of precipitation (NCP runs) effectively suppresses cold pools (Fig. 6a), but moisture aggregation is still a common feature (Fig. 6d). Without cold pools, the thermodynamic structure of the simulated atmosphere is significantly different (Fig. 7). While the amount of rain in the cloud layer differs only little (Fig. 7a), surface precipitation is higher in the NCP runs than in the STD runs (see also Fig. 6e). This is attributable to the fact that in the NCP runs all the rain reaches the surface, while in the STD runs, a large fraction evaporates during its fall through the subcloud layer

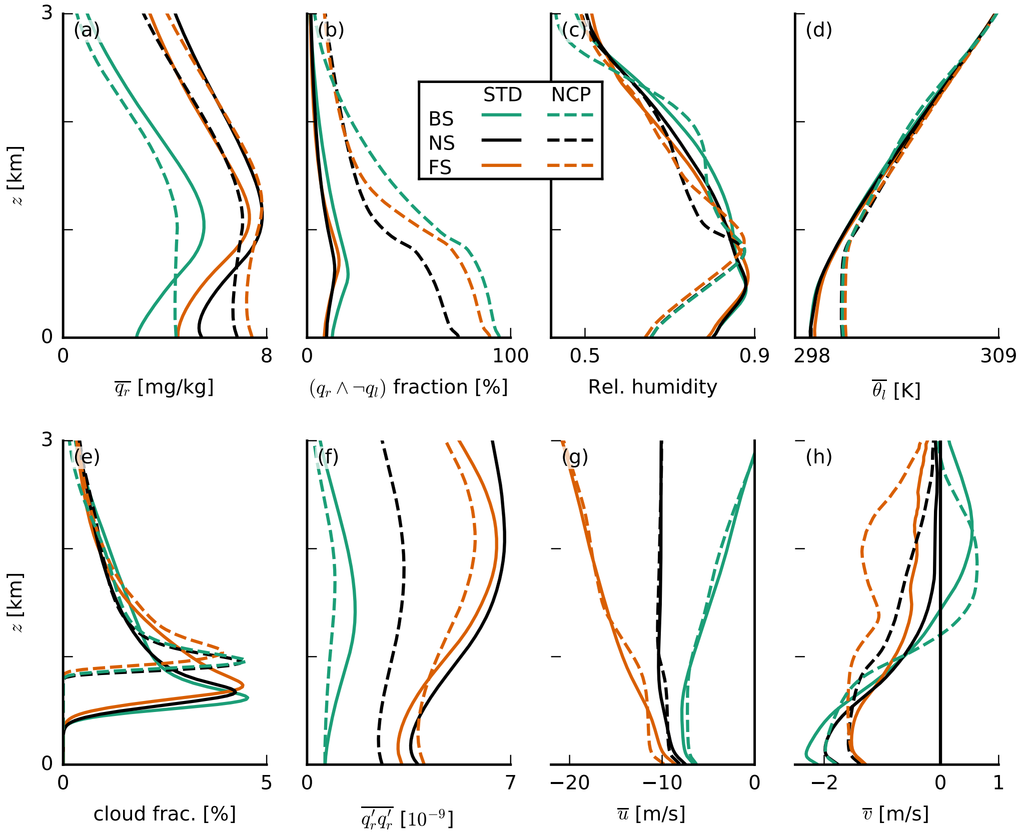

Figure 7: Slab-averaged profiles of (a) rain water specific humidity q_r, (b) the ratio of rainy grid points outside of clouds, (c) relative humidity, (d) liquid water potential temperature θ_l, (e) cloud fraction, (f) the variance of q_r, (g) zonal wind speed u and (h) meridional wind speed v, all averaged over the last ten hours of each simulation.

(Fig. 7a). Consequently, more grid points outside of clouds contain rain in the NCP runs than in the STD runs (Fig. 7b), while within clouds, the ratio is unchanged (not shown). The lack of rain evaporation in the subcloud layer leads to a decreased relative humidity there (Fig. 7c). This is caused by both the lack of transfer of rain water to water vapour and by the lack of evaporative cooling, which results in a warmer subcloud layer (Fig. 7d). The result is a higher cloud-base height (Fig. 7e) and a deeper mixed layer, for example evident in the temperature, relative-humidity and zonal wind profiles (Fig. 7c, d, g).

Without evaporation of precipitation and thus cold pools, cloud tops are not significantly lower, but convective deepening is delayed by some extent (Fig. 6b–c). Already in the first 12 h of the simulation, we notice a tendency of the FS case to develop on average somewhat deeper clouds (Fig. 6b) and to produce larger mesoscale moisture aggregation (Fig. 6d), suggesting that this case has some additional advantage over the NS and BS cases that is unrelated to cold pools. In the next section, we focus on convective behaviour in the NCP runs as well as in the early stages of development of the STD runs.

4.2 Convective structure along the shear vector

Exemplary snapshots of cloud systems from the NCP simulations (Fig. 8) suggest that under FS and NS, precipitation is falling downwind from the clouds and downwind from the subcloud-layer roots of the clouds where new updrafts and clouds develop. Under BS, precipitation tends to fall vertically into the existing subcloud-layer updraft, leading to an inhibition of further convective development from that root.

We can attempt to quantify where in the various shear cases rain shafts are located in relation to the bulk of the clouds and liquid water. We can organize the domain by column-integrated water vapour (CWV), where high CWV corresponds to regions where moisture converges to form (deep) clouds. In some sense, mapping all grid points by CWV allows us to create a cross section through the bulk water vapor and cloud structure, moving from clear sky regions (low CWV) to cloud centers (high CWV). Figure 9 shows how precipitation is distributed as a function of height and CWV. The shear cases have somewhat different distributions of CWV, but nonetheless, differences in the distribution of rain are visible. Under NS and even more under FS, the presence of rain in columns with lower CWV is evident, whereas under BS, rain water below clouds is limited to the columns with highest CWV.

The difference in the CVW-binned cloud and rain distributions do not reveal whether rain is located upwind or downwind of clouds. To quantify the precipitation's preferred direction with respect to the clouds, we perform an analysis of the cross-correlation of the cloud-water field with the rain-water field. The cross-correlation is a measure for the similarity of two vectors as a function of shift relative to each other, which is commonly used in signal processing. Generally, the cross-correlation of two discrete real functions f and g of length N is defined by:

$$X(\Delta) = \sum_{j=0}^{N} f(j)g(j+\Delta), \tag{1}$$

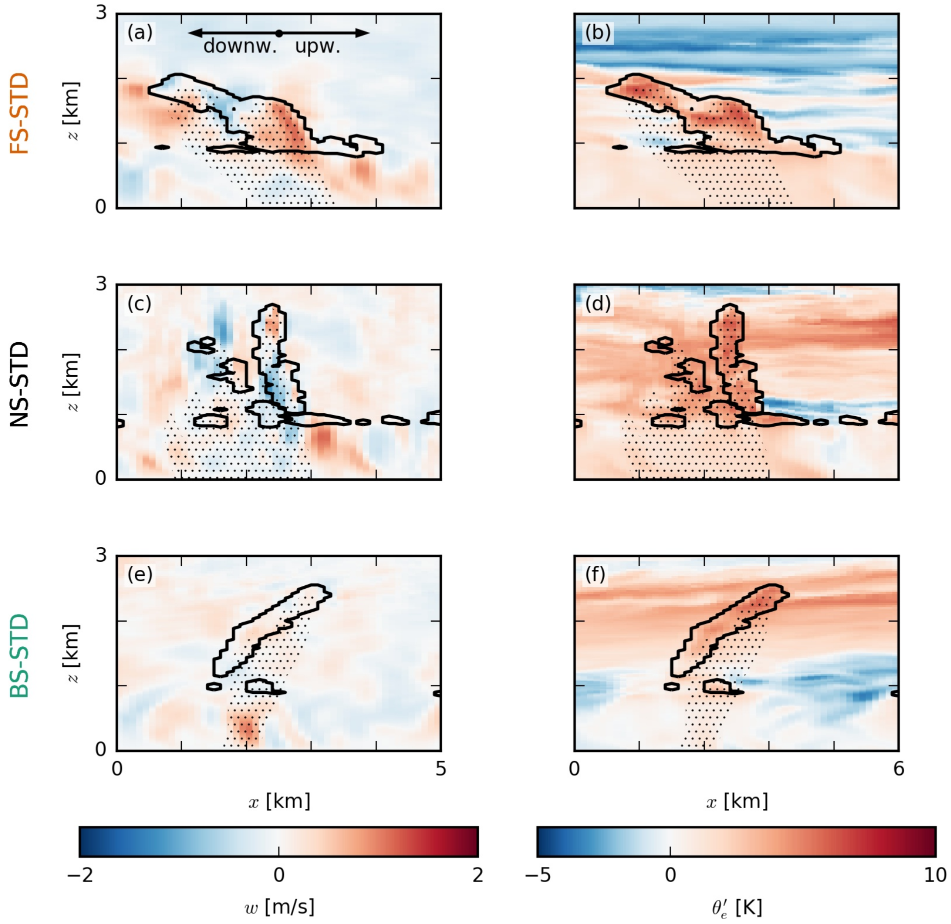

Figure 8: Snapshots of exemplary clouds in the (a–b) FS-NCP, (c–d) NS-NCP and (e–f) BS-NCP cases. The colourmaps in the x-z slices show (left column) the vertical velocity w and (right column) the equivalent potential temperature anomaly θ_e. Just as Fig. 3, the black outlines indicate clouds (i.e. the $q_l = 0$ isoline), and the dotted areas indicate precipitation. Each panel is 5 km wide, averaged over 1 km in the meridional direction and taken from the late stages of the simulation (around 40 h) to allow for a comparison with Fig. 3.

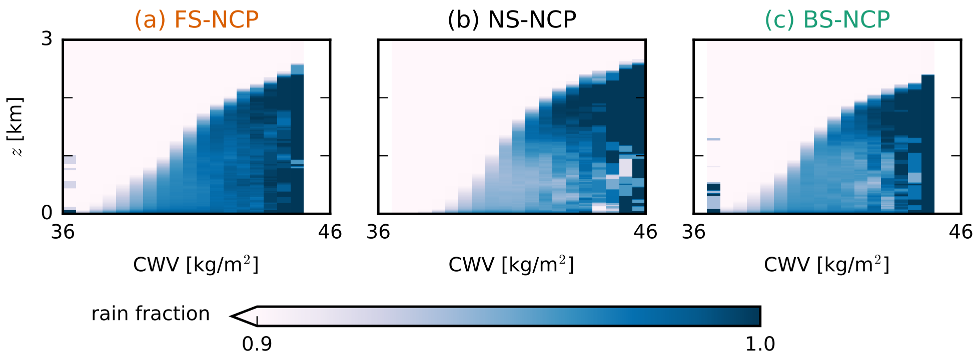

Figure 9: Composite profiles of the fraction of rainy grid points ($q_r > 0$) averaged over bins of column-integrated water vapour (CWV). All data are averaged from 30-minute output of the instantaneous 3D fields in the hours 12–18 of the NCP simulations.

where Δ indicates the displacement (lag) of g with respect to f. We compute the cross-correlation of every row i of the q_l field (at 1 km, i.e. near cloud base) with every other row of the q_r field (averaged over the subcloud layer up to 1 km) and sum up the resulting vectors. Making use of the periodicity of the fields (i.e. $N+i \mathrel{\widehat{=}} i$), this yields a matrix,

$$X(\Delta_i, \Delta_j) = \sum_{i=0}^{N} \sum_{j=0}^{N} q_l(i,j) q_r(i+\Delta_i, j+\Delta_j), \tag{2}$$

with positive values where similarities between the two fields occur. The 'coordinates' (Δ_i, Δ_j) of the centre of mass of this matrix are assumed to form a good measure of the offset of the precipitation field with respect to the cloud field. The time series of these coordinates in Fig. 10 shows a clear signal in the first 24 h of the simulations, especially in the x-coordinate. During this time, there is a negative x-offset of the q_r field with respect to the q_l field in the FS and NS cases of up to 100 m (Fig. 10a). A negative offset here means downwind. In the BS case, however, the x-offset is much weaker and of inconsistent sign. Thus, in the FS and NS cases, rain falls down-wind of clouds, while in the BS case, precipitation is located under clouds. Shear tilts clouds (resulting in a higher projected cloud cover, see Fig. 6f), which causes part of the rain to fall out of the sides of the clouds: downwind under FS and upwind under BS (as visible in Fig. 8). On the second day, the convection becomes more clustered and less random and the offset signal thus more inconsistent. The y-offset is more random (Fig. 10b), but this is not surprising given that the mean wind is in the zonal direction.

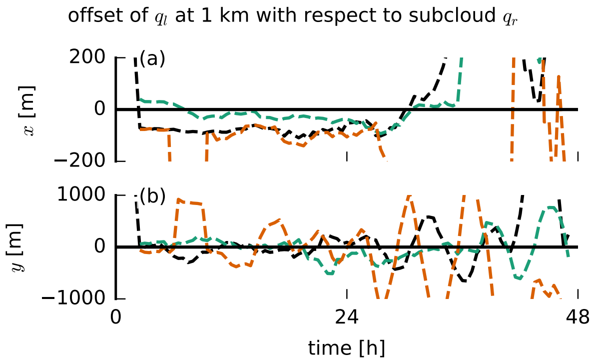

Figure 10: Lateral offset in (a) x and (b) y of the rain water specific humidity field averaged over 0–1 km with respect to the liquid water specific humidity field at 1 km. The offset is computed from the centre of mass of the matrix that contains the sum of the cross-correlation vectors of each row of the q_l field with every other row of the q_r field (Eq. 2). The analysis is done on 30-minute output of the instantaneous 3D fields. For clarity, we only show the NCP simulations here.

The tendency of new updrafts to emerge upwind of existing clouds in the FS and NS cases (see Fig. 8) is because the subcloud layer is characterised by zonal forward shear (Fig. 7g). This means that clouds move faster than their roots (subcloud-layer thermals), which literally stay behind and form new clouds upwind of the cloud. In the BS case, there is only little shear in the subcloud layer, and the wind speed is similar near the ground and at cloud base. This implies that the roots of thermals move at the same speed as the clouds above, making them more vulnerable to precipitative downdrafts.

5 Discussion and conclusion

In this paper, we used idealised LES experiments with and without cold pools and with different amounts of vertical wind shear, to investigate how cloud morphology and the structure of cold pools influence convective development and deepening. We summarise our findings in the schematic in Fig. 11. In the BS case, two effects inhibit cloud development and thus also cloud deepening and organisation (including the formation of cold pools):

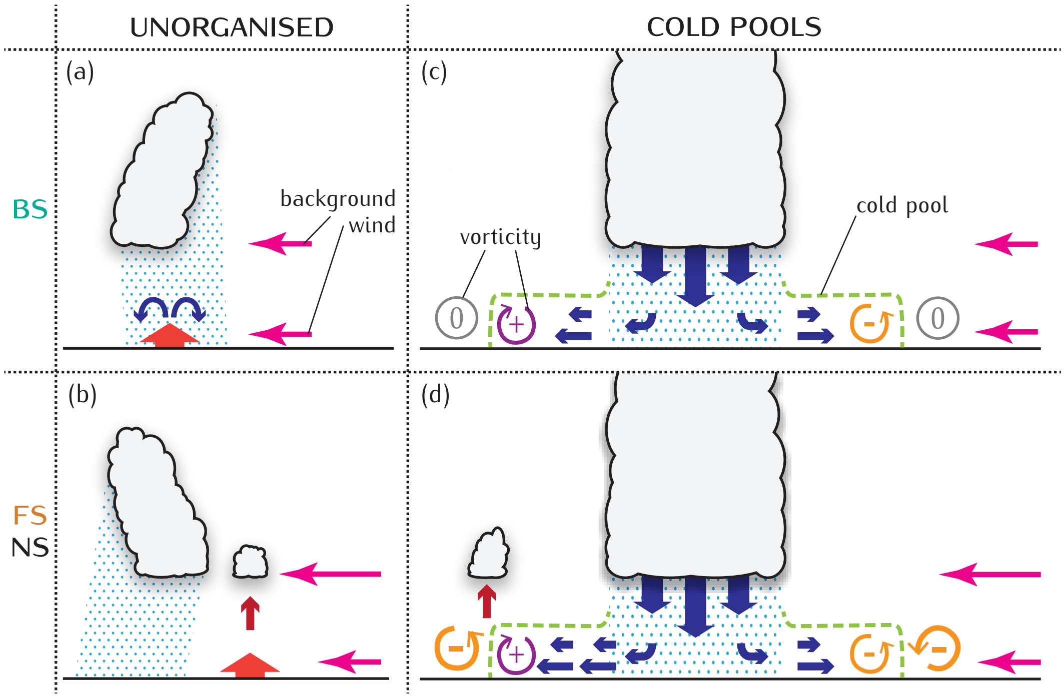

Figure 11: Conceptual picture of (a–b) the morphology of unorganised clouds and (c–d) the structure of cold pools in (a, c) the BS case, on the one hand, and (b, d) the FS and NS cases, on the other hand.

1. Precipitative downdrafts are located at the same location as or upwind in relation to existing clouds, which is also where new updrafts tend to form (Fig. 11a). The precipitation hence hampers new and existing convective cells in their development.
2. If cold pools are present, the subcloud-layer wind profile does not form a favourable region of opposite vorticity at cold-pool fronts (Fig. 11c) as it does under FS and NS. In the latter cases, the subcloud-layer is characterised by forward shear, which implies the presence of negative vorticity, which interacts with the downwind cold-pool front which has positive vorticity to trigger additional lifting at this position (Fig. 11d).

The second mechanism of cold pool-induced convection may only occur to limited extent in the present FS case, although surface precipitation (Fig. 5f and 6e) and the strength of downdrafts (Fig. 5c) are of similar magnitude in the FS and the NS cases. Cold pools in the FS case are less vigorous because precipitation is spread out over larger areas, as reflected in the similar variance of q_r in the FS-STD and FS-NCP cases (Fig. 7f): In the NS case, the variance of q_r significantly increases (while q_r itself only increases slightly) from the NCP to the STD case, i.e. when convection transforms from more random organisation with precipitation throughout the domain (low variance) to cold pools with narrow strong rain shafts and dry areas surrounding them (high variance). In the FS case, the variance does not significantly increase, suggesting that even though convection is deep enough to produce large amounts of precipitation (Fig. 6c, e), the strong shear spreads precipitation out over a larger area (Fig. 9a), preventing cold pools from forming (Fig. 6a). Moreover, the fact that precipitative downdrafts are located downwind of clouds may form a disadvantage in this phase of the simulation because this is also where secondary convection is triggered (see Fig. 3a).

As a result of the inhibited cloud development, moisture aggregation under BS occurs much later and clouds remain shallower for a longer period in contrast to FS and NS (Fig. 6b–d). Once strong precipitative downdrafts lead to the formation of cold pools, the relocation of convective triggering to locations upwind instead of downwind diminishes the disadvantage of the BS case. Conversely, under FS and NS, the spatial separation between updrafts and precipitative downdrafts appears beneficial for sustaining the thermal circulations that aid cloud development and may also let emerging updrafts benefit from a pre-moistened environment ahead of them. However, once rain starts falling at the same downwind location where cold pools trigger new convection (see Fig. 3a), the tendency of the FS case to deepen and rain more in the early stages of the STD simulation (and form more cold pools) ceases.

Overall, the cloud morphology is thus most favourable for convective deepening if forward shear is present in the subcloud layer (FS and NS cases) but not in the cloud layer (BS case). In the cloud layer, any absolute shear weakens cloud updrafts and thus convective deepening by increasing the downward oriented pressure perturbation force (HNRS20). Together, these two findings explain why cloud tops are lower in both the present shear cases compared to the NS case, but less so under FS. In the BS case, shear both in the subcloud layer and in the cloud layer is disadvantageous for cloud deepening, while in the FS case, only the cloud-layer shear forms a disadvantage.

In addition to the role of wind shear in the dynamic triggering of secondary convection at cold-pool gust fronts (Li et al., 2014), we show that shear also makes a difference for convective development before cold pools are present. The use of constant surface enthalpy fluxes does not appear to be a strong counter-argument to that conclusion, as interactive surface fluxes are only of importance for cold pools over land (Gentine et al., 2016). Furthermore, HNRS20 showed that simulations with interactive surface fluxes have a similar response to wind shear as those with constant surface fluxes, and, in fact, preliminary analysis suggests that this is also the case for the cold-pool characteristics presented here. Overall, our results suggest that cold pools over sea enhance congestus systems (which occur even without them), but are not the underlying reason for convective deepening.

Acknowledgments

We would like to thank Paquita Zuidema for inspiring discussions on cold-pool dynamics and Simon Schneider for instructive explanations of the cross-correlation. This project has received funding from the European Research Council (ERC) under the European Union's Horizon 2020 research and innovation programme (Starting grant agreement no. 714918). DALES is open-source software, which is distributed under the terms of the GNU GPL version 3. The exact version of the code as well as the input files used in this work are available via `https://doi.org/10.5281/zenodo.4668479`.

References

Böing, S. J., Jonker, H. J. J., Siebesma, A. P., & Grabowski, W. W. (2012). Influence of the Subcloud Layer on the Development of a Deep Convective Ensemble. *Journal of the Atmospheric Sciences*, *69*(9), 2682–2698. doi: 10.1175/JAS-D-11-0317.1

Bony, S., Schulz, H., Vial, J., & Stevens, B. (2020). Sugar, Gravel, Fish, and Flowers: Dependence of Mesoscale Patterns of Trade-Wind Clouds on Environmental Conditions. *Geophysical Research Letters*, *47*(7), 1–9. doi: 10.1029/2019GL085988

Bony, S., Stevens, B., Frierson, D. M. W., Jakob, C., Kageyama, M., Pincus, R., ... Webb, M. J. (2015). Clouds, circulation and climate sensitivity. *Nature Geoscience*, *8*(4), 261–268. doi: 10.1038/ngeo2398

Daleu, C. L., Woolnough, S. J., & Plant, R. S. (2012). Cloud-Resolving Model Simulations with One- and Two-Way Couplings via the Weak Temperature

Gradient Approximation. *Journal of the Atmospheric Sciences*, *69*(12), 3683–3699. doi: 10.1175/JAS-D-12-058.1

Gentine, P., Garelli, A., Park, S. B., Nie, J., Torri, G., & Kuang, Z. (2016). Role of surface heat fluxes underneath cold pools. *Geophysical Research Letters*, *43*(2), 874–883. doi: 10.1002/2015GL067262

Grabowski, W. W. (1998). Toward Cloud Resolving Modeling of Large-Scale Tropical Circulations: A Simple Cloud Microphysics Parameterization. *Journal of the Atmospheric Sciences*, *55*(21), 3283–3298. doi: 10.1175/1520-0469(1998)055⟨3283:TCRMOL⟩2.0.CO;2

Grant, L. D., Moncrieff, M. W., Lane, T. P., & Heever, S. C. (2020). Shear-Parallel Tropical Convective Systems: Importance of Cold Pools and Wind Shear. *Geophysical Research Letters*, *47*(12), 1–10. doi: 10.1029/2020GL087720

Helfer, K. C., Nuijens, L., de Roode, S. R., & Siebesma, A. P. (2020). How Wind Shear Affects Trade-wind Cumulus Convection. *Journal of Advances in Modeling Earth Systems*, *12*(12). doi: 10.1029/2020MS002183

Heus, T., van Heerwaarden, C. C., Jonker, H. J. J., Siebesma, A. P., Axelsen, S., van den Dries, K., ... Vilà-Guerau de Arellano, J. (2010). Formulation of the Dutch Atmospheric Large-Eddy Simulation (DALES) and overview of its applications. *Geoscientific Model Development*, *3*(2), 415–444. doi: 10.5194/gmd-3-415-2010

Holland, J. Z., & Rasmusson, E. M. (1973). Measurements of the Atmospheric Mass, Energy, and Momentum Budgets Over a 500-Kilometer Square of Tropical Ocean. *Monthly Weather Review*, *101*(1), 44–55. doi: 10.1175/1520-0493(1973)101⟨0044:MOTAME⟩2.3.CO;2

Khairoutdinov, M., & Randall, D. (2006). High-resolution simulation of shallow-to-deep convection transition over land. *Journal of the Atmospheric Sciences*, *63*(12), 3421–3436. doi: 10.1175/JAS3810.1

Kurowski, M. J., Suselj, K., Grabowski, W. W., & Teixeira, J. (2018). Shallow-to-Deep Transition of Continental Moist Convection: Cold Pools, Surface Fluxes, and Mesoscale Organization. *Journal of the Atmospheric Sciences*, *75*(12), 4071–4090. doi: 10.1175/JAS-D-18-0031.1

Li, Z., Zuidema, P., & Zhu, P. (2014). Simulated convective invigoration processes at trade wind cumulus cold pool boundaries. *Journal of the Atmospheric Sci-*

ences, *71*(8), 2823–2841. doi: 10.1175/JAS-D-13-0184.1

Mahoney, K. M., Lackmann, G. M., & Parker, M. D. (2009). The Role of Momentum Transport in the Motion of a Quasi-Idealized Mesoscale Convective System. *Monthly Weather Review*, *137*(10), 3316–3338. doi: 10.1175/2009MWR2895.1

Nuijens, L., & Siebesma, A. P. (2019). Boundary Layer Clouds and Convection over Subtropical Oceans in our Current and in a Warmer Climate. *Current Climate Change Reports*, *5*(2), 80–94. doi: 10.1007/s40641-019-00126-x

Peters, J. M., Hannah, W., & Morrison, H. (2019). The Influence of Vertical Wind Shear on Moist Thermals. *Journal of the Atmospheric Sciences*, *76*(6), 1645–1659. doi: 10.1175/JAS-D-18-0296.1

Rotunno, R., Klemp, J. B., & Weisman, M. L. (1988). A Theory for Strong, Long-Lived Squall Lines. *Journal of the Atmospheric Sciences*, *45*(3), 463–485. doi: 10.1175/1520-0469(1988)045⟨0463:ATFSLL⟩2.0.CO;2

Schlemmer, L., & Hohenegger, C. (2014). The Formation of Wider and Deeper Clouds as a Result of Cold-Pool Dynamics. *Journal of the Atmospheric Sciences*, *71*(8), 2842–2858. doi: 10.1175/JAS-D-13-0170.1

Schulz, H., Eastman, R., & Stevens, B. (2021, in review). Characterization and Evolution of Organized Shallow Convection in the Trades. *Journal of Geophysical Research*. doi: 10.1002/essoar.10505836.1

Seifert, A., & Heus, T. (2013). Large-eddy simulation of organized precipitating trade wind cumulus clouds. *Atmospheric Chemistry and Physics*, *13*(11), 5631–5645. doi: 10.5194/acp-13-5631-2013

Stevens, B., Bony, S., Brogniez, H., Hentgen, L., Hohenegger, C., Kiemle, C., . . . Zuidema, P. (2019). Sugar, gravel, fish and flowers: Mesoscale cloud patterns in the trade winds. *Quarterly Journal of the Royal Meteorological Society*, *146*(726), 141–152. doi: 10.1002/qj.3662

Stevens, B., Bony, S., Farrell, D., Ament, F., Blyth, A., Fairall, C., . . . Zöger, M. (2021, in review). EUREC^{4}A. *Earth System Science Data Discussions*. doi: 10.5194/essd-2021-18

Tompkins, A. M. (2001). Organization of Tropical Convection in Low Vertical Wind Shears: The Role of Cold Pools. *Journal of the Atmospheric Sciences*, *58*(13), 1650–1672. doi: 10.1175/1520-0469(2001)058⟨1650:OOTCIL⟩2.0.CO;2

Torri, G., Kuang, Z., & Tian, Y. (2015). Mechanisms for convection triggering by cold pools. *Geophysical Research Letters*, *42*(6), 1943–1950. doi: 10.1002/2015GL063227

Weisman, M. L., & Rotunno, R. (2004). “A Theory for Strong Long-Lived Squall Lines” Revisited. *Journal of the Atmospheric Sciences*, *61*(4), 361–382. doi: 10.1175/1520-0469(2004)061⟨0361:ATFSLS⟩2.0.CO;2

Xue, H., Feingold, G., & Stevens, B. (2008). Aerosol Effects on Clouds, Precipitation, and the Organization of Shallow Cumulus Convection. *Journal of the Atmospheric Sciences*, *65*(2), 392–406. doi: 10.1175/2007JAS2428.1